SmartMat

WILEY

SmartMat Open Access

RESEARCH ARTICLE OPEN ACCESS

A Highly Ductile Composite of 3D-Printed Poly(Lactic Acid) With InSe Particles and Flakes as a Filler

Huihui Li[1,2] | Zhongliang Yu[1,3] | Bowen Liu[1,4] | Yang Gao[1,4] | Ming Liu[1,4] | Jianqi Zhang[1,4] | Rodney S. Ruoff[5,6,7,8] | Bin Wang[1,4,5]

[1]CAS Key Laboratory of Nanosystem and Hierarchical Fabrication, National Center for Nanoscience and Technology (NCNST), Beijing, China | [2]Tianjin Key Laboratory of Molecular Optoelectronic Sciences, Department of Chemistry, School of Sciences, Tianjin University, Tianjin, China | [3]College of Mechanical Engineering, Yangzhou University, Yangzhou, China | [4]University of Chinese Academy of Sciences, Beijing, China | [5]Center for Multidimensional Carbon Materials (CMCM), Institute for Basic Science (IBS), Ulsan, Republic of Korea | [6]Department of Chemistry, Ulsan National Institute of Science and Technology (UNIST), Ulsan, Republic of Korea | [7]Department of Materials Science and Engineering, Ulsan National Institute of Science and Technology (UNIST), Ulsan, Republic of Korea | [8]School of Energy and Chemical Engineering, Ulsan National Institute of Science and Technology (UNIST), Ulsan, Republic of Korea

Correspondence: Zhongliang Yu (zlyu@yzu.edu.cn) | Rodney S. Ruoff (rsruoff@ibs.re.kr; ruofflab@gmail.com) | Bin Wang (wangb@nanoctr.cn)

Received: 30 April 2024 | **Revised:** 19 June 2024 | **Accepted:** 23 June 2024

Funding: This work was supported by the National Key R&D Program of China (2021YFA1202802), the Institute for Basic Science (IBS-R019-D1; R.S.R.), the Natural Science Foundation of China (12102098), the China Postdoctoral Science Foundation Funded Project (2020M680479, 2021M690801), and the CAS Pioneer Hundred Talents Program.

Keywords: 3D printing | InSe | PLA composites | strength | toughness

ABSTRACT

The biodegradable polymer poly(lactic acid) (PLA) is brittle. PLA-based composites reinforced by indium selenide (InSe) particles or flakes are prepared; each is found to have outstanding plasticity. InSe nanosheets are prepared by sonication of solid InSe in *N*-methyl pyrrolidone, followed by washing/dispersion in ethanol, and subsequent drying. These InSe nanosheets, or in separate studies InSe particles, are mixed with PLA to make composite materials. The PLA composite materials are 3D-printed into "dogbone" samples that are tensile-loaded. The optimum dogbone specimen is 1.5 times stronger and 5.5 times tougher than neat PLA specimens prepared in the same way. To the best of our knowledge, this concurrent improvement in tensile strength and toughness has not been achieved before in PLA with any filler type. Finite element analysis, together with experimental analysis of (i) fracture surfaces, (ii) the PLA crystal structure, and (iii) the internal structure by micro-CT scanning, suggests that the exceptional mechanical performance is due to the intrinsic properties of InSe and, particularly, the emergence of crack shielding and crack deflection at the interfaces of PLA and InSe flakes. These findings indicate that PLA–InSe composites may offer opportunities to broaden the applications of PLA composites, including as load-bearing materials.

1 | Introduction

Poly(lactic acid) (PLA) is a biodegradable polymer that has great potential for use in packaging, medical instruments, automotive, and other applications [1–3]. However, there is a crucial deficiency of PLA that impedes its application as a structural material, that is, the intrinsic brittle response (i.e., catastrophic failure) when subjected to mechanical loading [4]. See Supporting Information S1: Figure S1, which shows its brittleness when bent or stretched. It is reported that the ductility and toughness of PLA could be improved by blending with a plasticizer or fibrils, such as poly (ethylene octene) (POE) [5],

The first two authors contributed equally to this article.

or poly (butylene adipate-co-terephthalate) (PBAT) [6], or polytetrafluoroethylene (PTFE) [7]. The reported increases in ductility of those PLA composites came at the "expense" of lowered strength. For instance, He et al. [5] recently reported that incorporating POE into PLA yielded an improvement of 226% for the elongation at break; yet, the strength of the composite was reportedly decreased by more than 30% as compared with the neat PLA.

Achieving improvements in both strength and toughness has been a long-standing challenge in the mechanics of composites [8]. The appearance of two-dimensional (2D) [9–14] and one-dimensional (1D) [15–19] nanomaterials has provided new options to explore this challenge. For instance, Seligra et al. [16] reported that PLA with carbon nanotubes (CNTs) modified by benzoyl chloride showed higher strength and toughness than neat PLA (1.1× strength and 1.3× toughness). Wang et al. [18] reportedly used surface modification and worm-like helical CNTs as fillers in an attempt to improve interfacial interaction and thus the toughness of PLA composites while maintaining their strength. Graphene nanoplates have been used to reinforce PLA, and the reported strength and toughness were improved by 1.4× and 1.9×, respectively [20]. However, the inherently low plasticity of graphene [21] or inferior interface compatibility between the PLA matrix and the fillers used to date, we suggest, limits further improvement of strength and toughness of PLA-based composites.

Indium selenide (InSe), an inorganic 2D van der Waals material, has widespread applications in optoelectronics, photodetectors, and field-effect transistors [22–24]. Compared with CNTs, graphene, and other common fillers, InSe has superplastic deformability and Young's modulus in the range of 30–50 GPa, two orders of magnitude lower in stiffness [25–28]. This exceptional mechanical property of InSe primarily stems from its intralayer pliability and significant interlayer deformable sliding. This observation inspires the consideration of InSe as a filler for PLA, potentially offering a solution to mitigate PLA's brittleness. However, the mechanical properties of InSe-reinforced PLA and/or other polymer-based composites with InSe have not been reported, to the best of our knowledge.

Here, we report the reinforcement of PLA using InSe microparticles (named as InSe) and 2D InSe nanosheets (named as exfoliated InSe, E-InSe). The composites were formed into mechanical testing specimens by using 3D printing. To obtain E-InSe, we exfoliated the commercial InSe particles using a liquid-phase sonication method, and the β-phase crystal structure of 2D InSe remained unchanged. The E-InSe has a lateral size of about 200 nm and a thickness of about 3.8 nm. The InSe-based fillers endow PLA with 1.5× the strength and 5.5× the toughness in the optimum case, which considerably surpasses the reported factors of increase for PLA with CNTs and/or graphene as fillers. The strengthening and toughening are attributed to the high ductility of the InSe-based samples and the effect of the interface on crack shielding and crack deflection, based on our analysis of mechanical loading data, and finite element simulations. This work demonstrates that InSe fillers improve the mechanical properties, especially toughness, of PLA composites, which may broaden their commercial applications in many fields.

2 | Experiment

2.1 | Materials

The commercial PLA filament with a diameter of 1.75 mm was purchased from Aurora Technology Co. Ltd., China. InSe powder with a purity of 99.999% was supplied by Alfa Metal Materials Co. Ltd., China. The *N*-methyl-2-pyrrolidone (NMP) solvent (Reagent Grade, 99%) was purchased from Sinopharm Chemical Regent Co. Ltd., China. Dichloromethane, ethanol, and isopropanol (IPA) were all Reagent Grade (99%) and were provided by Beijing Dongfang Shibo Fine Chemical Co. Ltd., China.

2.2 | Preparation of Reinforcements and PLA-Based Composites

The nano-size InSe reinforcements were achieved by liquid-phase exfoliation (LPE) of InSe particles. First, pristine InSe particles were added to NMP (6.25 mg/mL). Then, the suspension was ultrasonicated at a power of 180 W and in a flowing water bath (20°C–40°C) to avoid a dramatic increase of temperature. After sonication for 12 h, the dispersion was transferred to a centrifuge tube and centrifuged at 2000 r/min for 45 min. The collected supernatant was filtered in an attempt to remove NMP and the obtained InSe was transferred into ethanol as a solvent (or dispersant). Finally, this dispersion was evaporated and the E-InSe flakes were then obtained. Note that the optimum conditions mentioned above for exfoliation of InSe were determined by exploring the following parameters: the exfoliation solvent, the ultrasonic intensity, and the duration of sonication. As shown in Supporting Information S1: Figure S2, the obtained samples had a certain morphology and size at an ultrasonic power of 180 W and sonication time of 12 h at a concentration of 6.25 mg/mL in an NMP solvent. Graphene oxide (G-O) was used as a control sample for reinforcement, and the graphite oxide that was then exfoliated to G-O was synthesized using the modified Hummers' method.

The PLA composite samples that were mechanically loaded to determine their mechanical response were prepared using the 3D printing method as shown in Figure 1A. First, the PLA filament was dissolved in dichloromethane by stirring and heating to 50°C. Different fillers (InSe, E-InSe, and G-O) were separately dispersed in ethanol by ultrasonication in a water bath; this filler dispersion was then mixed with the PLA/dichloromethane solution. This mixture would evaporate and transform into a composite viscous "mud" after heating under stirring. Then, the mud was poured into a glass culture dish until it evaporated completely, ultimately forming a composite film with a thickness of approximately 1 mm.

An extrusion-based 3D printing method was used to fabricate the composites. Like the direct ink writing process at low temperatures, the raw materials loaded into a high-temperature syringe are heated to their melting point and then extruded at the predetermined pressure. The underlying theory of this 3D printing technology is akin to fused deposition modeling (FDM) 3D printing. Fabrication of nanocomposite specimens is more convenient, as it eliminates the need for a filament. The bio-3D printer (3D-BioplotterTM Envision TEC GmbH, Germany), equipped with two printing syringes (a low-temperature one

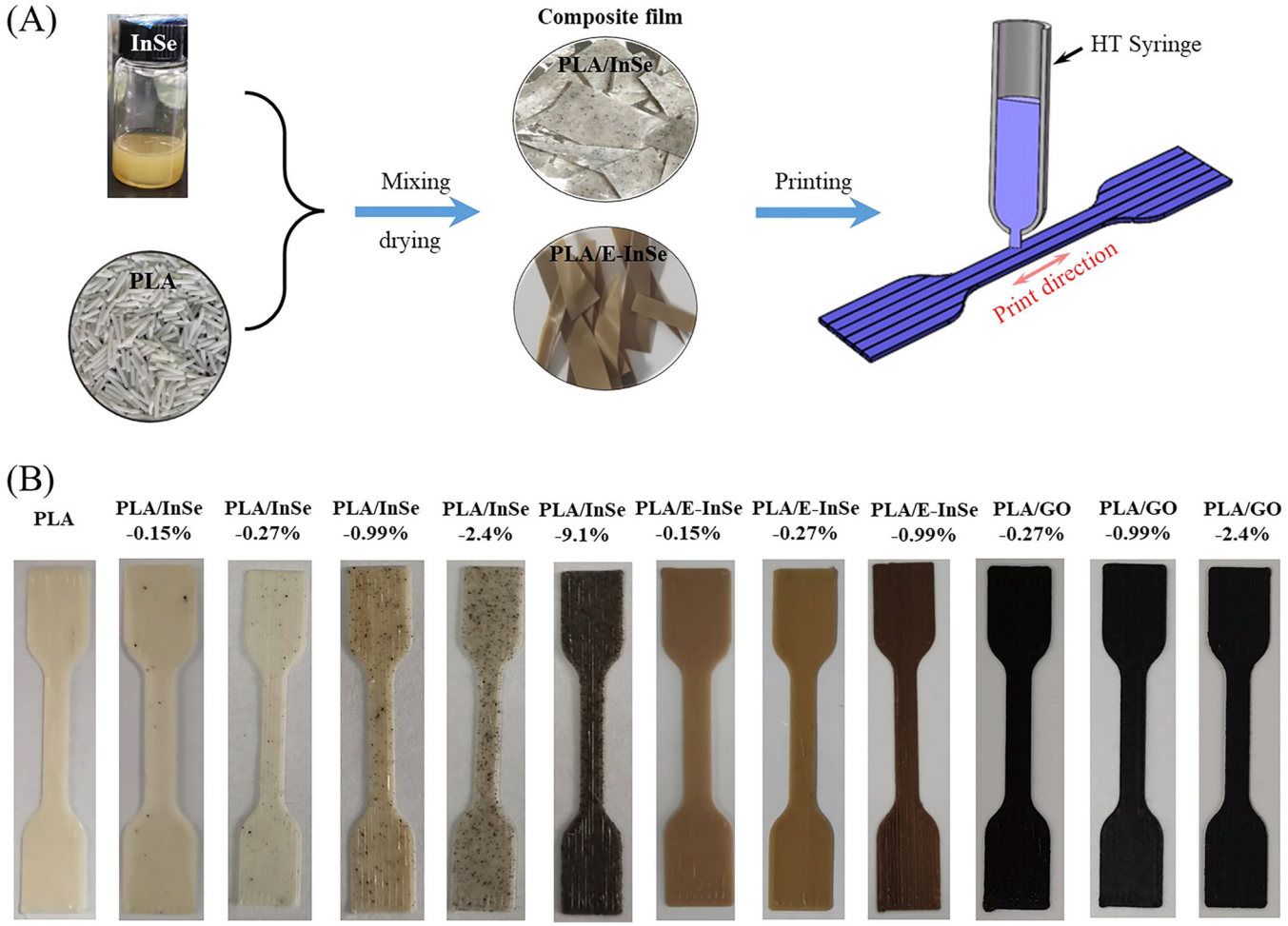

FIGURE 1 | Preparation of the PLA composites as tensile-test specimens. (A) Schematic for preparing exfoliated InSe (E-InSe) and, ultimately, 3D-printed composites as dogbone specimens. HT denotes high temperature. (B) Photos of the printed specimens.

and a high-temperature one) and a movement resolution of ~1 μm, has been extensively utilized to fabricate a wide array of materials, ranging from soft hydrogels to hard ceramics and polymers. Here, we adeptly utilize this printer to fabricate the PLA/InSe nanocomposites.

As shown in Figure 1A, the composite film was cut into small fragments and loaded into the high-temperature printing syringe of the printer. Throughout the printing process, four crucial factors—printing temperature, printing platform temperature, dosing pressure, and printing speed—need meticulous adjustment to produce high-quality samples devoid of voids and accumulations. Supporting Information S1: Table S1 comprehensively details the 3D printing conditions for each composite. We believe that other researchers can replicate our processes and results using a similar 3D printer or an FDM printer.

We then printed dogbone tensile specimens with a gauge length of 12 mm, a width of 2.0 m, and a thickness of 0.25 mm, of each of pure PLA, PLA/InSe composites with four different weight percentages of InSe particles, PLA/E-InSe composites with two weight percentages of InSe flakes, and PLA/G-O composites with three weight percentages of G-O. The width and thickness of each printed sample were measured by SEM before the tensile testing. The composites are named as PLA/RT-*N*, in which RT denotes the filler and *N* is the weight percentage of the filler. Thus, PLA/InSe-0.27% denotes composites consisting of 0.27 wt% InSe and 99.73 wt% PLA. Photos of all the printed dogbone specimens are shown in Figure 1B.

3 | Results and Discussion

3.1 | Morphology and Crystal Structure of the Fillers

We optimized the LPE process, and the obtained E-InSe samples are shown in Figure 2A and Supporting Information S1: Figure S2 (the detailed preparation can be found in the Supporting Information). The pristine InSe particles with sizes of tens of microns show irregular steps on their surfaces, indicating the lamellar structure that enables the possibility of exfoliation. The inset in Supporting Information S1: Figure 2A highlights an E-InSe with an in-plane size of ~400 nm. Our statistical analysis shows that the lateral sizes of E-InSe are mainly in the range of 160–220 nm (see Figure 2B). The thickness was measured to be ~3.8 nm based on atomic force microscopy (AFM), as per the image in Figure 2C, indicating that the E-InSe sheet contains four layers (with a monolayer thickness of 0.9 nm [29]). The high-resolution transmission electron microscopy (TEM) image in Figure 2D shows a lattice spacing of 0.34 nm that

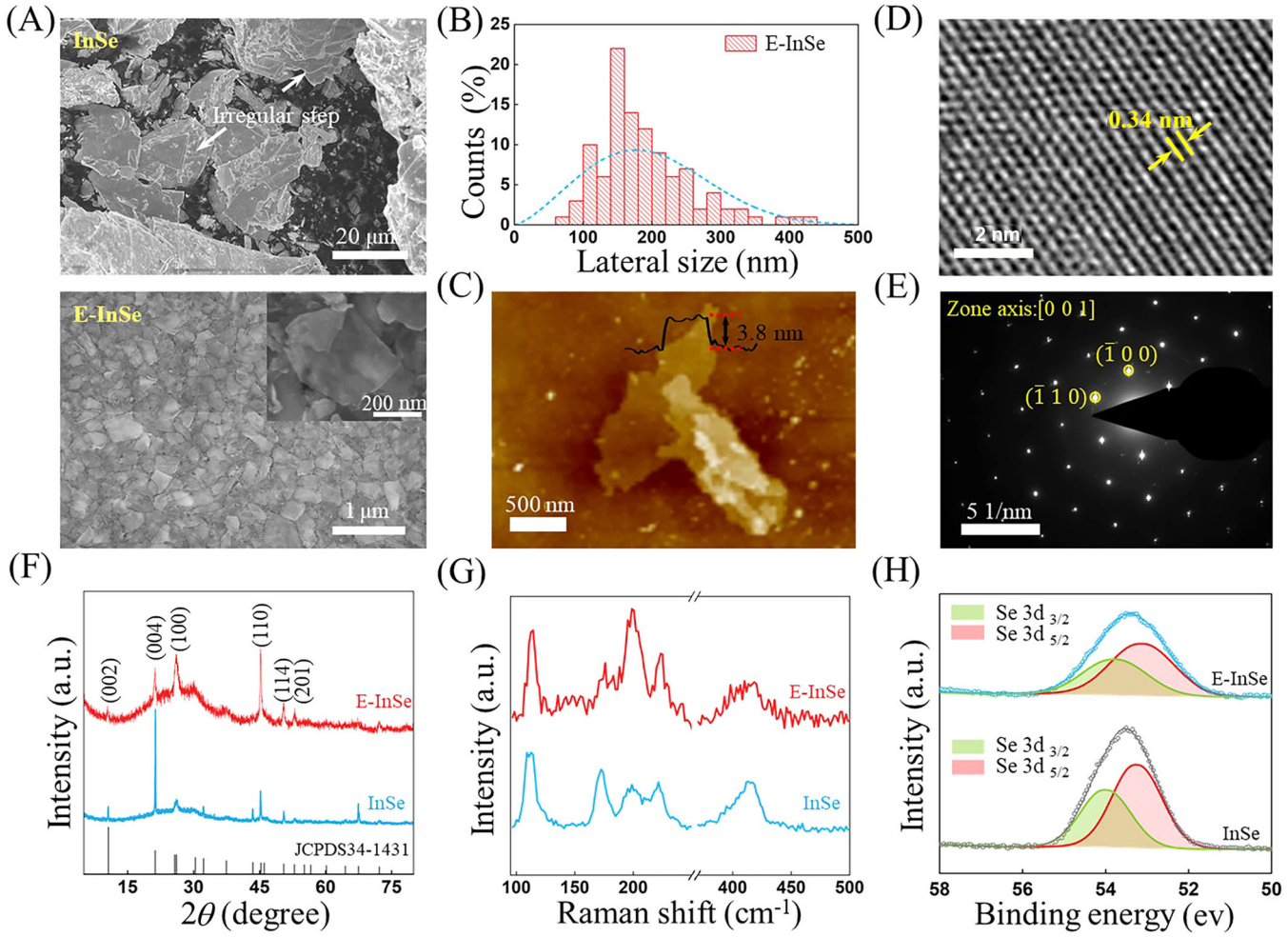

FIGURE 2 | Characterization of exfoliated InSe nanosheets (E-InSe). (A) Comparison in SEM morphology of pristine InSe particles (InSe) and E-InSe. (B) Plot of lateral size versus number observed, for E-InSe. (C) AFM analysis of an E-InSe flake, with the height profile of the nanosheet shown. (D) High-resolution TEM image and (E) SAED pattern of E-InSe. The plots for (F) XRD, (G) Raman spectra, and (H) XPS show the characteristic diffraction peaks (XRD) and spectra (Raman and XPS) of β-InSe.

could correspond to the (101) plane of InSe or of In_2Se_3, but the selected electron diffraction (SAED) pattern in Figure 2E shows that the material studied here is pure InSe [25]. X-ray diffraction (XRD) was performed for InSe and E-InSe (Figure 2F), and the observed peaks match β-InSe (JCPDS34-1431). β-InSe belongs to the hexagonal lattice system and the P63/mmc space group. It has active vibrational modes that appear in the Raman spectrum, as shown in Figure 2G, in agreement with the reported analyses [29, 30]. The acquired X-ray photoelectron spectroscopy (XPS) spectra of InSe and E-InSe show the characteristic peaks of β-InSe corresponding to Se 3d and In 3d core levels (see Figure 2H and Supporting Information S1: Figure S4A). The related morphological and compositional characterizations for G-O (also used as a filler for a comparison study) are shown in Supporting Information S1: Figure S4.

3.2 | Mechanical Behavior of PLA Composites

We conducted uniaxial tensile tests on the composites and obtained stress–strain curves, as shown in Figure 3A and Supporting Information S1: Figure S5. Each thick curve in Figure 3A is the calculated average from three curves (three separate tests) of one composite. The pristine PLA showed an almost linear elastic response and then brittle fracture at a strain of 5.1%–5.7%, and adding G-O nanosheets to the PLA matrix yielded a similar stress–strain response. PLA composites with only 0.27 wt% InSe filler (either InSe particles or flakes) showed outstanding plasticity with softening and plastic flow following the elastic deformation, as well as higher strength, stiffness, and failure strain, than the neat PLA and PLA/G-O composites.

We analyzed the strength, stiffness, ductility, and toughness of all the composites with their different mass fractions and fillers (see Figure 3B,C and Supporting Information S1: Table S2). The strength and stiffness of the PLA matrix increased with the addition of the InSe particle filler. However, when the filler loading reached 9.1 wt%, the excessive InSe particles induced significant stress concentration, resulting in decreased mechanical properties. In comparison with PLA/InSe-0.27%, PLA/E-InSe-0.27% composites showed a higher strength: 45.8 ± 1.9 versus 41.7 ± 3.7 MPa (the detailed strengthening mechanism is discussed later). Compared to pure PLA (average strength of 32.2 MPa and stiffness of 749.4 MPa), the optimum PLA-based composites with 0.27 wt% InSe showed a 42.3%

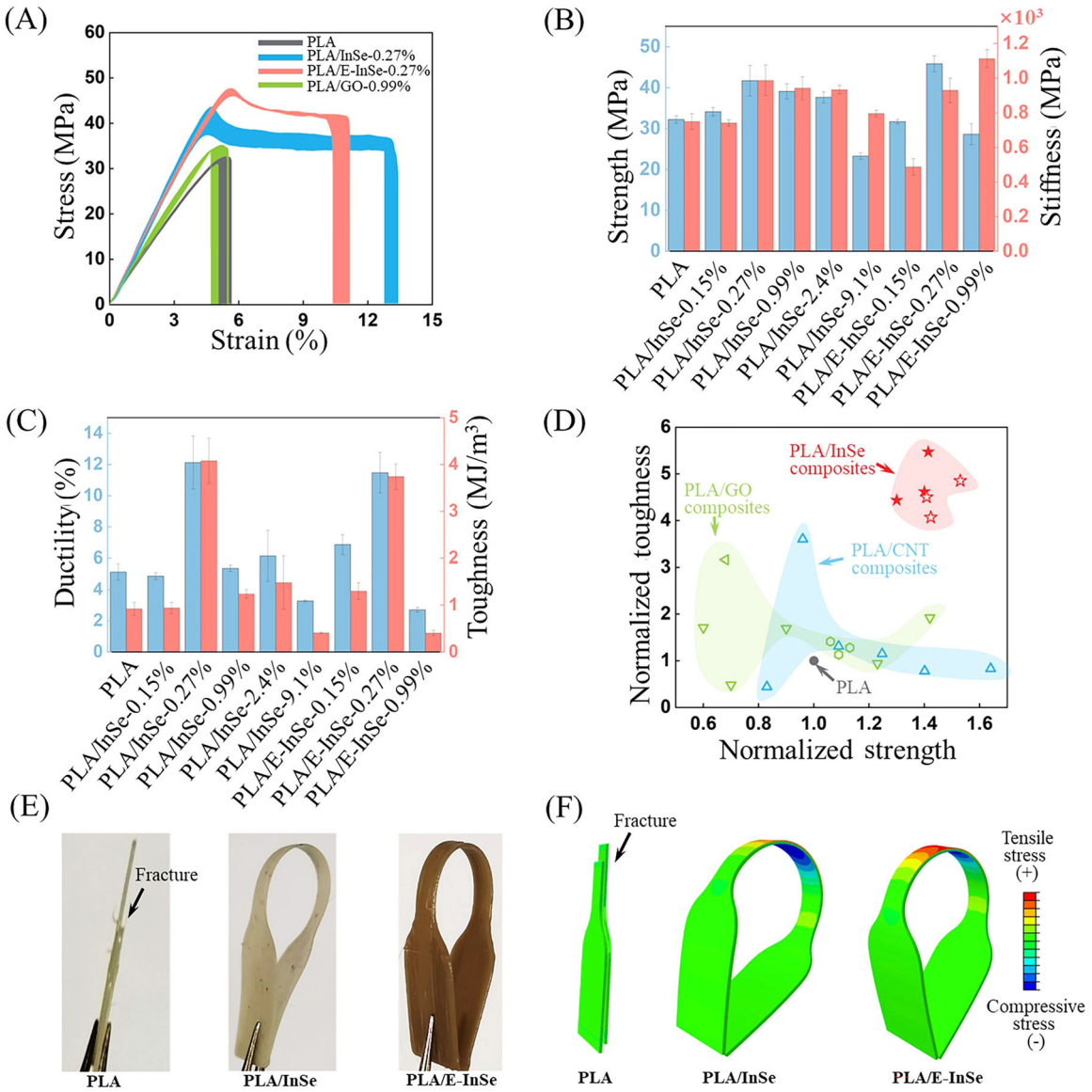

FIGURE 3 | Mechanical properties of the PLA composites. (A) Tensile stress–strain curves of four representative kinds of composites. Each thick curve in the figure is the average of three curves for different specimens of one composite type. (B) The histograms highlight that both InSe and E-InSe can increase the strength and stiffness of composites simultaneously, where PLA/E-InSe shows a higher average strength. (C) The plots show that the composites with only 0.27 wt% pristine InSe particles have the optimum ductility and toughness, slightly higher than that containing E-InSe. (D) Compared with the related reported mechanics for PLA composites with other filler types, both PLA/InSe and PLA/E-InSe composites have higher strength and toughness. The solid stars show data of PLA/InSe and the hollow stars show data for PLA/E-InSe composites. The three hexagons show the testing data of PLA/GO samples prepared in this work, whereas the triangles show the data from the literature. The flexibility of neat PLA, PLA/InSe, and PLA/E-InSe composites is shown by (E) bending the specimens and from a simulation (F).

increase in strength, whereas the optimal PLA-based composites with 0.99 wt% E-InSe shows a 48.5% increase in stiffness. Embedding either InSe or E-InSe into the PLA matrix also yielded higher ductility and toughness, that is, on average 2.4× and 2.2× the ductility, and 4.4× and 4.1× the toughness for InSe- and E-InSe-reinforced PLA, respectively, when compared with that of PLA (Figure 3C). The increased strength and toughness might result from the interfacial interaction between InSe and PLA as well as the inherent ultra-large plasticity of InSe [28] (see the detailed explanation later).

The normalized strength and toughness of PLA/InSe and PLA/E-InSe composites (normalized by the strength and toughness of PLA in every case to exclude the effects of raw materials and testing conditions) are compared with those of CNT- and G-O-reinforced composites (The detailed data for the reported results and this work in Figure 3D are listed in Supporting Information S1: Table S3 [9, 11, 15–18, 20, 31–33].). The reported PLA/CNT and PLA/G-O composites show either improved strength or toughness. For instance, PLA composites filled with the surface-modified helical CNT showed 3.6× the toughness of the neat PLA, but without strength enhancement [18]. The control samples of PLA/G-O specimens prepared in this work showed 1.1× the strength and 1.1×– 1.4× the toughness of neat PLA, whereas the optimal InSe-based fillers yielded 1.5× the strength and 5.5× the toughness. The PLA/E-InSe composites showed

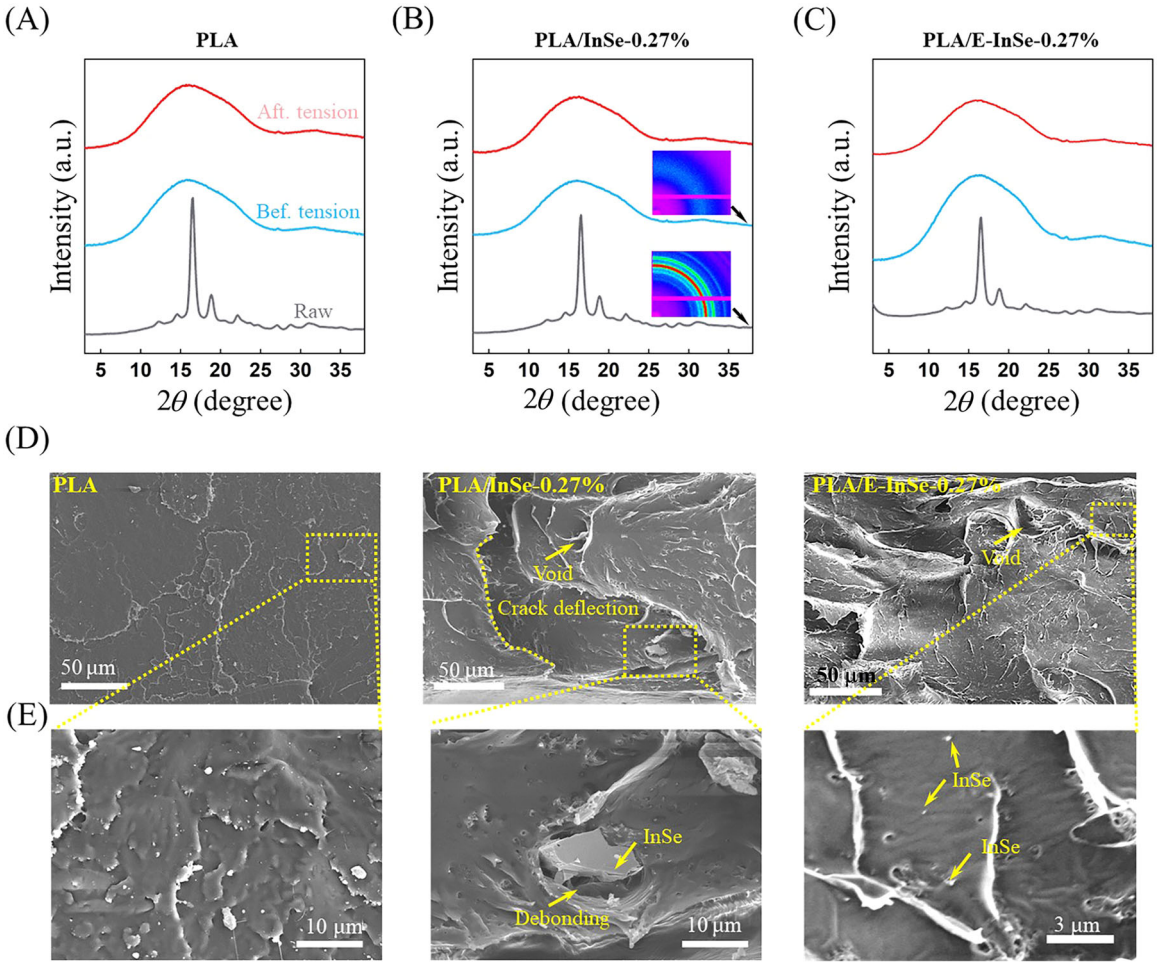

FIGURE 4 | Analysis of strengthening and toughening mechanisms. WAXS characterization for (A) neat PLA, (B) PLA/InSe-0.27%, and (C) PLA/E-InSe-0.27%. The inset indicates the 2D mapping of the diffraction patterns. (D) Fracture analysis of the tested tensile composites by investigating the morphology of the fractured surfaces using SEM (D, E).

the highest average strength of 45.8 MPa, whereas the PLA/InSe composites showed the highest average toughness of 4.1 MJ/m^3 among all the control samples. The combination of excellent mechanical and optical characteristics in PLA/InSe composites expands their potential applications in specialized packaging fields requiring UV insensitivity (Figure S6) and load-bearing capability.

Bent specimens show the flexibility of PLA/InSe and PLA/E-InSe composites; see Figure 3E. Brittle fracture in the PLA and PLA/G-O composites occurred readily when one end of the tensile specimen was bent to attach the other end (Supporting Information S1: Figure S7). In contrast, both the PLA/InSe and PLA/E-InSe composites never failed at the same bending strain, showing exceptional deformability. The bending simulation was performed using the commercial ABAQUS/standard v.6.12 software. The PLA/InSe and PLA/E-InSe composites were considered as isotropic homogeneous materials and their effective material properties were extracted from the stress–strain curves in Figure 3A. When the tensile specimens are bent, the outer surface is in tensile stress and the inner surface is under compressive stress. The increasing stress with continuous bending leads to the brittle fracture of the neat PLA, whereas the PLA/InSe and PLA/E-InSe composites show macroscopic plasticity.

3.3 | Strengthening Mechanism and Toughening Mechanism

It is reported that either the transition of crystalline PLA to an amorphous phase [34] or nanocrystalline PLA formation/growth [35] can lead to its brittle–ductile transition. We investigated the crystal structures of the tensile specimens with wide-angle X-ray scattering (WAXS). As shown in Figure 4A, all the raw PLA materials before 3D printing are crystalline but transformed into amorphous after melting and extrusion from the 3D printing nozzle. InSe and E-InSe fillers did not vary the crystallization of PLA (Figure 4B,C). PLA/InSe-0.27% and PLA/E-InSe-0.27% composites in the segment subjected to the large plastic deformation were still amorphous after the tension, that is, thus in agreement with the reported absence of strain-induced crystallization [36]. Therefore, the mechanical enhancement of PLA from InSe or E-InSe is not due to changes in the structure of the PLA matrix. The fillers InSe or E-InSe, and the interfaces between them and PLA, are thus perhaps the key factors.

The postmortem fracture surfaces of three kinds of specimens were observed by SEM (Figure 4D,E). For the neat PLA, the main crack quickly penetrates the whole sample after the crack nucleates, resulting in a smooth fracture surface. However, the

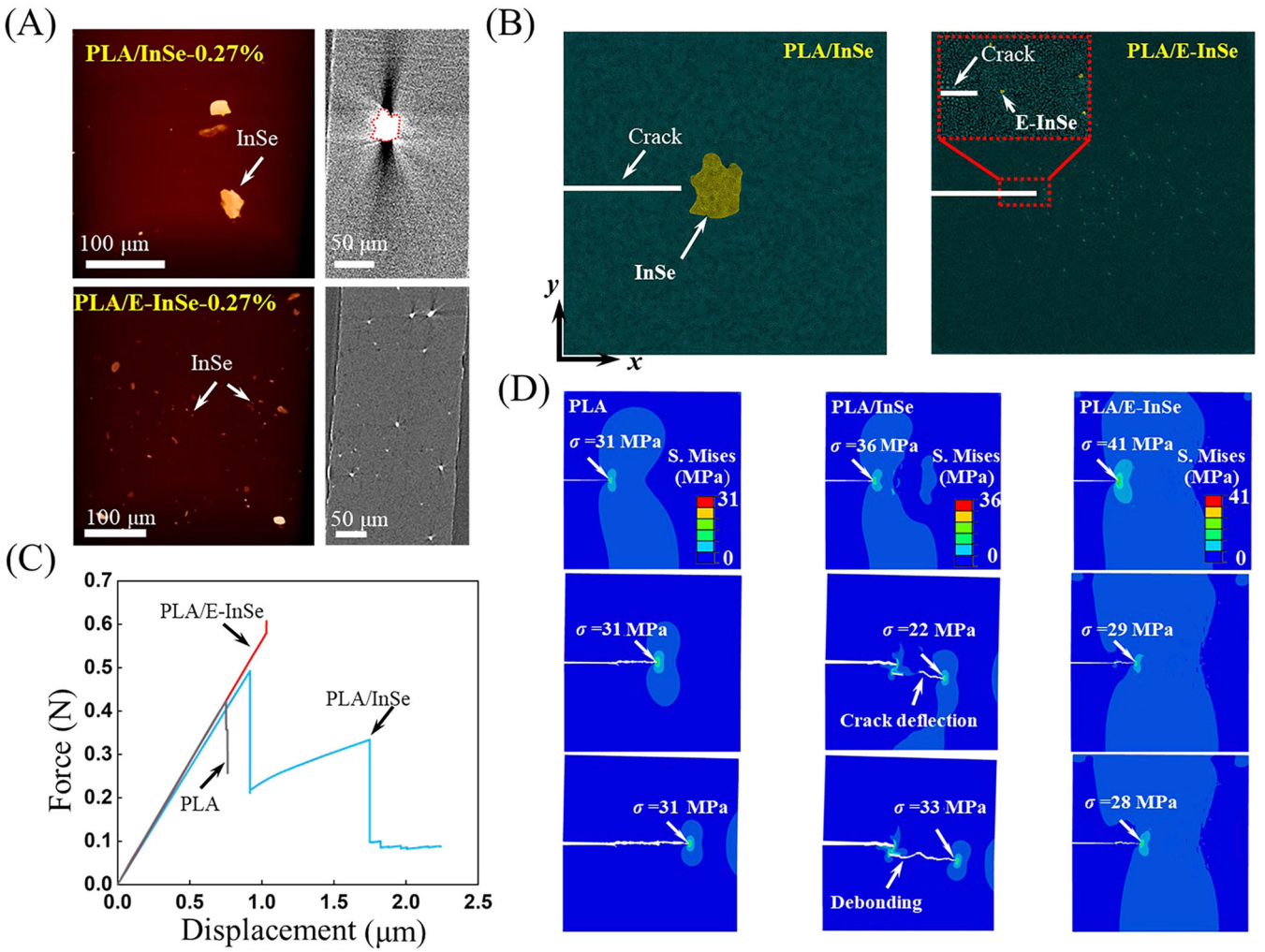

FIGURE 5 | Finite element analysis to study reinforcement mechanisms. (A) CT scanning images show the spatial distributions of the InSe particles and E-InSe flakes. The gray images denote the 2D sectional morphology and the others show 3D morphology. (B) Simplified 2D model for simulation. The profile of InSe is depicted according to the CT images in (A). (C) Comparison of force–displacement curves for neat PLA, PLA/InSe, and PLA/E-InSe composites. (D) Mises stress distributions and crack propagation trajectory in these three composites; σ is the maximum Mises stress at the crack tip.

observed InSe-induced interface debonding and the formation of voids might have led to the ductile failure fracture surface in both PLA/InSe and PLA/E-InSe composites. It has been reported that interface debonding and voids arising from crack defection and bifurcation can cause enhanced toughness in composites [37–39].

Microcomputed tomography (CT) Scanning images were used to observe the dispersion of InSe particles and E-InSe flakes in the 3D-printed PLA composites (Figure 5A). Within the same size range, the E-InSe flakes show a higher number density than the InSe particles, implying the formation of more interfaces with the PLA matrix (Supporting Information S1: Figure S9). Based on the "2D section" morphology of CT scanning, we set up the PLA/InSe and PLA/E-InSe composite models for finite element analysis (FEA) (Figure 5B). The size of each model is 0.2 mm × 0.2 mm, and the length of the pre-crack is 0.05 mm. The profile of InSe was obtained by digitizing the 2D CT images and the E-InSe with the same mass fraction was randomly arranged in the matrix. To simulate the damage and fracture of the PLA matrix, the build-in ductile damage model in ABAQUS/standard v.6.12 was adopted and the properties of the material were incorporated by fitting the tensile testing data in Figure 3A, which includes the intrinsic mechanical properties of the fillers. The InSe was assumed to be a linear material with Young's modulus of 28 GPa according to the reported nano-indentation testing [25]. The mechanical response of the interface between PLA and InSe was treated using the interfacial cohesive zone model, which estimates the interfacial damage and failure through a traction–separation relationship. The detailed material parameters are listed in Supporting Information S1: Table S4.

For performing the calculation, the bottom surface was fixed in the *y*-direction and the top surface was uniformly loaded with a fixed displacement. Other surfaces are traction-free. The force applied on the composites was recorded as the displacement increases, as shown in Figure 5C, which indicates that the neat PLA fractures catastrophically and yet, the PLA/InSe composites still have load-bearing capability to withstand increasing force after the first loading drops. We were not able to obtain the complete force–displacement curve for the PLA/E-InSe due to the computational convergence problem, but it still shows a larger maximum force than PLA.

The corresponding crack nucleation and propagation are shown in Figure 5D. The crack in PLA directly grows along the pre-crack direction with the permanent crack driving force (i.e., the same crack tip stress). However, with InSe particles distributed in the PLA matrix, the stress field around the crack tip is continuously redistributed as the crack propagates owing to interfaces between the PLA matrix and the particles [37]. As a result, the crack driving force is attenuated and the composite recovers the load-bearing capacity due to crack shielding and blunting, resulting in the second rising force in Figure 5C. Crack deflection was also observed and the interface would de-bond as the load increased, which dissipates extensive energy to toughen the material. Further, we investigated the effect of interfacial properties on the mechanical response of PLA/InSe composites. As a case study, two interfacial materials with differing fracture energies (strong interface/weak interface = 10) were simulated, while maintaining the same interfacial strength. Supporting Information S1: Figure S10 demonstrates that PLA/InSe composites with a strong interface show high resistance to interfacial debonding, resulting in improved toughness and higher secondary maximum bearing stress. In comparison with the PLA/InSe composites, the stress in PLA/E-InSe can be distributed throughout a larger region as of the many more particle–PLA interfaces, yielding more effective load transfer between E-InSe and PLA that delays local deformation and failure [40, 41], yielding higher strength than that for the InSe fillers. The reduced crack shielding during crack propagation for PLA/E-InSe may explain its lower toughness than the PLA composite with InSe particles as fillers. Overall, the PLA/InSe and PLA/E-InSe composites show higher strength and toughness due to the intrinsic properties of InSe and E-InSe along with interfacial debonding/crack deflection effects (Figure 5D).

4 | Conclusions

InSe particles and flakes were used as fillers and PLA as the matrix, and the resulting composites had significantly increased strength and toughness. The composites were 3D-printed to fabricate dog-bone specimens for tensile testing. The tensile and bending experiments indicate that PLA composites with InSe or E-InSe (nanosheets) undergo plastic deformation rather than brittle fracture in contrast to the neat PLA, PLA/G-O, and the reported PLA/CNT and PLA/G-O composites. Strength increase of 1.5× and 5.5× in toughness compared with the neat PLA was achieved. The PLA/InSe composite with 0.27 wt% fillers has higher toughness but lower strength than PLA/E-InSe. Surface fracture morphology and finite element simulations illustrate that the strengthening and toughening are due to the intrinsic deformability of InSe materials, as well as certain events that occur during fracture, including interface debonding, the formation of voids, and crack deflection and shielding. We suggest that these PLA/InSe composites can greatly broaden the use of PLA in load-bearing applications.

Acknowledgments

This work was supported by the National Key R&D Program of China (2021YFA1202802), the Institute for Basic Science (IBS-R019-D1; R.S.R), the Natural Science Foundation of China (12102098), the China Postdoctoral Science Foundation Funded Project (2020M680479, 2021M690801), and the CAS Pioneer Hundred Talents Program.

Conflicts of Interest

The authors declare no conflicts of interest.

Data Availability Statement

The data that support the findings of this study are available in the Supporting Information of this article.

References

1. L. T. Lim, R. Auras, and M. Rubino, "Processing Technologies for Poly (Lactic Acid)," *Progress in Polymer Science* 33, no. 8 (2008): 820–852.

2. F.-L. Jin, R.-R. Hu, and S.-J. Park, "Improvement of Thermal Behaviors of Biodegradable Poly(Lactic Acid) Polymer: A Review," *Composites, Part B: Engineering* 164 (2019): 287–296.

3. S. Liu, S. Qin, M. He, D. Zhou, Q. Qin, and H. Wang, "Current Applications of Poly(Lactic Acid) Composites in Tissue Engineering and Drug Delivery," *Composites, Part B: Engineering* 199 (2020): 108238.

4. A. P. Mathew, K. Oksman, and M. Sain, "Mechanical Properties of Biodegradable Composites From Poly Lactic Acid (PLA) and Microcrystalline Cellulose (MCC)," *Journal of Applied Polymer Science* 97, no. 5 (2005): 2014–2025.

5. W. He, L. Ye, P. Coates, F. Caton-Rose, and X. Zhao, "Reactive Processing of Poly(Lactic Acid)/Poly(Ethylene Octene) Blend Film With Tailored Interfacial Intermolecular Entanglement and Toughening Mechanism," *Journal of Materials Science & Technology* 98 (2022): 186–196.

6. S. Su, M. Duhme, and R. Kopitzky, "Uncompatibilized PBAT/PLA Blends: Manufacturability, Miscibility and Properties," *Materials* 13, no. 21 (2020): 4897.

7. J. Chai, G. Wang, A. Zhang, et al., "Ultra-Ductile and Strong In-Situ Fibrillated PLA/PTFE Nanocomposites With Outstanding Heat Resistance Derived by CO_2 Treatment," *Composites, Part A: Applied Science and Manufacturing* 155 (2022): 106849.

8. R. O. Ritchie, "The Conflicts Between Strength and Toughness," *Nature Materials* 10, no. 11 (2011): 817–822.

9. X.-Z. Tong, F. Song, M.-Q. Li, X.-L. Wang, I.-J. Chin, and Y.-Z. Wang, "Fabrication of Graphene/Polylactide Nanocomposites With Improved Properties," *Composites Science and Technology* 88 (2013): 33–38.

10. P. Liu, Z. Jin, G. Katsukis, et al., "Layered and Scrolled Nanocomposites With Aligned Semi-Infinite Graphene Inclusions at the Platelet Limit," *Science* 353, no. 6297 (2016): 364–367.

11. P.-P. Xu, S. Yang, X.-R. Gao, et al., "Constructing Robust Chain Entanglement Network, Well-Defined Nanosized Crystals and Highly Aligned Graphene Oxide Nanosheets: Towards Strong, Ductile and High Barrier Poly(Lactic Acid) Nanocomposite Films for Green Packaging," *Composites, Part B: Engineering* 222 (2021): 109048.

12. Y. Qian, C. Li, Y. Qi, and J. Zhong, "3D Printing of Graphene Oxide Composites With Well Controlled Alignment," *Carbon* 171 (2021): 777–784.

13. L. Peng, Y. Han, M. Wang, et al., "Multifunctional Macroassembled Graphene Nanofilms With High Crystallinity," *Advanced Materials* 33, no. 49 (2021): 2104195.

14. T. Liang and B. Wang, "Interlayer Covalently Enhanced Graphene Materials: Construction, Properties, and Applications," *Acta Physico Chimica Sinica* 38, no. 1 (2022): 2011059.

15. S. H. Park, S. G. Lee, and S. H. Kim, "Isothermal Crystallization Behavior and Mechanical Properties of Polylactide/Carbon Nanotube Nanocomposites," *Composites, Part A: Applied Science and Manufacturing* 46 (2013): 11–18.

16. P. G. Seligra, F. Nuevo, M. Lamanna, and L. Famá, "Covalent Grafting of Carbon Nanotubes to PLA in Order to Improve Compatibility," *Composites, Part B: Engineering* 46 (2013): 61–68.

17. R. Kotsilkova, I. Petrova-Doycheva, D. Menseidov, E. Ivanov, A. Paddubskaya, and P. Kuzhir, "Exploring Thermal Annealing and Graphene-Carbon Nanotube Additives to Enhance Crystallinity, Thermal, Electrical and Tensile Properties of Aged Poly(Lactic) Acid-Based Filament for 3D Printing," *Composites Science and Technology* 181 (2019): 107712.

18. Y. Wang, Y. Mei, Q. Wang, et al., "Improved Fracture Toughness and Ductility of PLA Composites by Incorporating a Small Amount of Surface-Modified Helical Carbon Nanotubes," *Composites, Part B: Engineering* 162 (2019): 54–61.

19. J. Li, H. Li, L. Xu, et al., "Biomimetic Nanoporous Aerogels From Branched Aramid Nanofibers Combining High Heat Insulation and Compressive Strength," *SmartMat* 2, no. 1 (2021): 76–87.

20. M. Kim, J. H. Jeong, J.-Y. Lee, et al., "Electrically Conducting and Mechanically Strong Graphene–Polylactic Acid Composites for 3D Printing," *ACS Applied Materials & Interfaces* 11, no. 12 (2019): 11841–11848.

21. C. Lee, X. Wei, J. W. Kysar, and J. Hone, "Measurement of the Elastic Properties and Intrinsic Strength of Monolayer Graphene," *Science* 321, no. 5887 (2008): 385–388.

22. Q. Zhao, P. Chen, D. Zheng, T. Wang, A. Castellanos-Gomez, and R. Frisenda, "Multifunctional Indium Selenide Devices Based on Van Der Waals Contacts: High-Quality Schottky Diodes and Optoelectronic Memories," *Nano Energy* 108 (2023): 108238.

23. Z. Ali, M. Mirza, C. Cao, et al., "Wide Range Photodetector Based on Catalyst Free Grown Indium Selenide Microwires," *ACS Applied Materials & Interfaces* 6, no. 12 (2014): 9550–9556.

24. D. Xu, J. Li, Y. Xiong, et al., "Fast and Direct Identification of SARS-CoV-2 Variants via 2D InSe Field-Effect Transistors," *InfoMat* 5, no. 2 (2023): e12398.

25. D. H. Mosca, N. Mattoso, C. M. Lepienski, et al., "Mechanical Properties of Layered InSe and Gase Single Crystals," *Journal of Applied Physics* 91, no. 1 (2002): 140–144.

26. Y. Li, C. Yu, Y. Gan, et al., "Elastic Properties and Intrinsic Strength of Two-Dimensional InSe Flakes," *Nanotechnology* 30, no. 33 (2019): 335703.

27. Q. Zheng, C. Liang, J. Jiang, and S. Li, "Elastic Properties and Deformation Mechanisms in the Van Der Waals Single-Crystalline Indium Selenide," *Physica Status Solidi (RRL)—Rapid Research Letters* 16, no. 3 (2022): 2100418.

28. T.-R. Wei, M. Jin, Y. Wang, et al., "Exceptional Plasticity in the Bulk Single-Crystalline Van Der Waals Semiconductor Inse," *Science* 369, no. 6503 (2020): 542–545.

29. N. Curreli, M. Serri, D. Spirito, et al., "Liquid Phase Exfoliated Indium Selenide Based Highly Sensitive Photodetectors," *Advanced Functional Materials* 30, no. 13 (2020): 1908427.

30. E. Petroni, E. Lago, S. Bellani, et al., "Liquid-Phase Exfoliated Indium–Selenide Flakes and Their Application in Hydrogen Evolution Reaction," *Small* 14, no. 26 (2018): 1800749.

31. L. S. D. Bortoli, R. Farias, D. Z. Mezalira, L. M. Schabbach, and M. C. Fredel, "Functionalized Carbon Nanotubes for 3D-Printed Pla-Nanocomposites: Effects on Thermal and Mechanical Properties," *Materials Today Communications* 31 (2022): 103402.

32. L. Yang, S. Li, X. Zhou, et al., "Effects of Carbon Nanotube on the Thermal, Mechanical, and Electrical Properties of PLA/CNT Printed Parts in the FDM Process," *Synthetic Metals* 253 (2019): 122–130.

33. C. Sriprachuabwong, S. Duangsripat, K. Sajjaanantakul, A. Wisitsoraat, and A. Tuantranont, "Electrolytically Exfoliated Graphene–Polylactide-Based Bioplastic With High Elastic Performance," *Journal of Applied Polymer Science* 132, no. 6 (2015): 41439.

34. S. Xu, J. F. Tahon, I. De-Waele, G. Stoclet, and V. Gaucher, "Brittle-to-Ductile Transition of PLA Induced by Macromolecular Orientation," *eXPRESS Polymer Letters* 14, no. 11 (2020): 1034–1047.

35. M. Razavi and S.-Q. Wang, "Why Is Crystalline Poly(Lactic Acid) Brittle at Room Temperature?," *Macromolecules* 52, no. 14 (2019): 5429–5441.

36. M. R. Mohamed Zin, A. Mahendrasingam, C. Konkel, and T. Narayanan, "Effect of *D*-Isomer Content on Strain-Induced Crystallization Behaviour of Poly(Lactic Acid) Polymer Under High Speed Uniaxial Drawing," *Polymer* 216 (2021): 123422.

37. W. Wang, K. Sadeghipour, and G. Baran, "Finite Element Analysis of the Effect of an Interphase on Toughening of a Particle-Reinforced Polymer Composite," *Composites, Part A: Applied Science and Manufacturing* 39, no. 6 (2008): 956–964.

38. J. G. Williams, "Particle Toughening of Polymers by Plastic Void Growth," *Composites Science and Technology* 70, no. 6 (2010): 885–891.

39. J. Gao, B. A. Patterson, Y. Kashcooli, D. O'Brien, and G. R. Palmese, "Synergistic Fracture Toughness Enhancement of Epoxy-Amine Matrices via Combination of Network Topology Modification and Silica Nanoparticle Reinforcement," *Composites, Part B: Engineering* 238 (2022): 109857.

40. S. Liu, J. Liu, Z. Xu, et al., "Artificial Bicontinuous Laminate Synergistically Reinforces and Toughens Dilute Graphene Composites," *ACS Nano* 12, no. 11 (2018): 11236–11243.

41. A. Bisht, S. S. Samant, S. Jaiswal, K. Dasgupta, and D. Lahiri, "Quantifying Nanodiamonds Assisted Exfoliation of Graphene and Its Effect on Toughening Behaviour of Composite Structure," *Composites, Part A: Applied Science and Manufacturing* 132 (2020): 105840.

Supporting Information

Additional supporting information can be found online in the Supporting Information section.